Pergamon

Int. J. Heat Mass Transfer. Vol. 40, No. 16, pp. 3937–3946, 1997

Printed in Great Britain
0017–9310/97 $17.00+0.00

PII: S0017–9310(97)00009–4

A numerical simulation of the solidification process of a binary mixture in a V-shaped enclosure

W. K. JONES, JR, S. E. DEZEGO, M. A. EBADIAN† and Z. F. DONG

Hemispheric Center for Environmental Technology, Florida International University, Miami, FL 33199, U.S.A.

(*Received* 24 *May* 1996 *and in final form* 26 *November* 1996)

Abstract—A numerical study of the solidification process for a eutectic forming aluminum–copper alloy in a V-shaped sump has been conducted. This geometry was chosen to simulate the limiting cases of sump angle (8° and 16°) for the physical domain of molten metal in the direct chill (DC) continuous casting process. The effects of melt convection and solid movement are also discussed as contributing factors to the segregation patterns. The results of the study showed the angle of the enclosure greatly affected negative segregation bands in the mushy region. Furthermore, the original negatively-segregated mushy zone gradually developed into a positively-segregated region throughout the solid area. © 1997 Elsevier Science Ltd.

1. INTRODUCTION

The continuous casting of metal alloys has developed into a dominant manufacturing process currently accounting for the production of at least 90% of all aluminum based ingots. The reasons for the increased application of continuous casting are the increased yield in product with a significant decrease in energy expended to produce the cast. The final alloy structure is greatly affected by the melt and cooling conditions, which, if not correctly controlled, can lead to species non-homogeneity within the ingot and non-uniform physical properties. Therefore, during the last three decades a great deal of research has been dedicated to understanding and improving the casting process.

Most of commercially produced metal alloys consist of at least two chemical components. Special consideration must be paid to these binary and ternary alloy systems inasmuch as the solidification occurs over a range of temperatures until the eutectic temperature has been reached. During the release of latent heat, these systems develop a characteristic two-phase region that is called the mushy zone. In eutectic-forming metal alloys, the mushy zone can be characterized as a varying-porosity dendritic structure. Due to the complexity of the solid–liquid interaction in this region, mathematical modeling has been slow to develop to unified theory describing both the micro and macro scale physical phenomena [1, 2]. The modeling of dynamic processing such as continuous casting is further complicated by the constant injection of super-heated, solute-rich material and the moving of the external boundaries of the caster walls.

In this process, melted material is poured into a water-cooled mold where solidification occurs due to heat rejection. After a starter billet of the alloy is formed, the dynamic process begins. The cooling jets impinging on the mold walls lowers the local temperature of the molten metal below its liquidus temperature, causing nucleation of equiaxed crystals in the molten metal. A columnar dendritic solid, attached to the cold wall, develops rapidly after nucleation. The solid front continues to grow perpendicular to the heat rejection and forms into a V-shape due to the downward progression of the mold walls. The angle of the V-shaped geometry is dependent on several factors, most notably the actuation speed of the caster and the heat flux generated by the cooling system. The angle has been experimentally verified to range from 8° to 16°. Recently, Burton *et al.* [3] experimentally investigated the phenomena that occurs in a 16° V-shaped sump. However, the conclusions were limited as to the effects the angle has on the solidification process and, more importantly, on the segregation of chemical species. Literature surveys have indicated that no investigations on the effect of the angle on the thermodynamic properties during solidification are available.

In this study, the solidification of a binary metal alloy is considered for a static, V-shaped sump that is symmetrically cooled below the eutectic temperature. Special consideration is given to the solution method due to the discontinuous geometry of the sump. The effects of solutal and thermal buoyancy forces, solid movement, and the variation of angle will be studied, being of primary interest is the resulting effects of these parameters on the macrosegregation, thermal profile, and flow patterns that develop during the solidification process in the V-shaped enclosure.

† Author to whom correspondence should be addressed.

NOMENCLATURE

A	interfacial area [m^2]
C	specific heat [J kg^{-1}-K^{-1}
c	concentration of solute
D	mass diffusion coefficient [m^2 s^{-1}]
d	mean particle length [m]
H	height of sump [m]
H	diffusional exchange coefficient
h	enthalpy [J]
I	interfacial term
k	thermal conductivity [W m^{-1}-K^{-1}]
k_p	equilibrium partition ratio
L	latent heat [J kg^{-1}]
m	volumetric solidification rate
p	pressure or isotropic stress tensor [N m^{-2}]
r	volume fraction
S	source term
T	temperature [K]
t	time [s]
T_m	fusion temperature [K]
u, v	velocities of x- and y-directions [m s^{-1}]
W	width of sump [m]
x, y	Cartesian coordinates.

Greek symbols

Δ	incremental time step [s]
ε	solid fraction
ϕ	phase variable
Γ	diffusion coefficient [kg m^{-3}-s^{-1}]
κ	segregation coefficient [wt% wt%]
μ	dynamic viscosity [kg m^{-1}-s^{-1}]
ρ	density [kg m^{-3}]

Subscripts

e	eutectic
ϕ	phase variable
i	interface
l	liquid
o	initial
s	solid
w	wall.

Superscripts

ϕ	phase variable
i	interface.

2. MATHEMATICAL FORMULATION

Solidification is considered within a vertical, two-dimensional, constant angle V-shaped mold, as shown in Fig. 1. All walls of the enclosure are impermeable. The boundary conditions for the enclosure are that non-cooling walls are adiabatic and the no-slip conditions were applied to all walls of the mold. Initially, the entire sump is insulated and contains a superheated binary mixture of temperature T_o and concentration $c_{1,0}^{Cu}$. At time $t = 0$, both vertical walls of the V-shaped geometry are brought to and maintained at temperature T_w, which is below the eutectic temperature, T_e.

The physical behavior of the solidification process is modeled through the use of a two-phase system of equations. This two-phase model is considerably more advanced as compared to the continuum model in handling physical phenomena that occur during alloy solidification for two reasons. Firstly, two sets of conservation equations are derived, one based on the liquid phase and one based on the solid phase. Secondly, local phase equilibrium is not imposed on the system of equations, which therefore allows for solutal and thermal undercooling to be modeled. However, implementation of two-phase modeling has been limited because the numerical techniques are not as widely accepted and a degree of uncertainty is associated with the modeling of the interfacial exchange terms. The equations presented below are based on the assumptions outline in ref. [4], where applicable.

In the present study, the liquid is treated as the first phase, whereas the solid is treated as the second phase, the region where both $0 < r_l < 1$ and $0 < r_s < 1$ correspond to the mushy (or two-phase) zone. All physical quantities, temperature, concentration, velocity, and so on are defined for both phases. Given that any value of a thermophysical property may vary between phases, velocity difference (slip) and thermal difference (undercooling) can be modeled to occur between phases. It is important to cast these equations in a general form that is consistent with the present numerical procedures. Therefore, a set of general governing equations of the form:

$$\frac{\partial}{\partial t}(\rho_l r_l \phi_l) + \nabla \cdot (\rho_l r_l u_l \phi_l) = \nabla \cdot (\Gamma_l^{\phi} \nabla \phi_l) + S_l^{\phi} + I_l^{\phi} \quad (1)$$

$$\frac{\partial}{\partial t}(\rho_s r_s \phi_s) + \nabla \cdot (\rho_s r_s u_s \phi_s) = \nabla \cdot (\Gamma_s^{\phi} \nabla \phi_s) + S_s^{\phi} + I_s^{\phi} \quad (2)$$

is required to describe the transport phenomena during alloy solidification. The variable ϕ could represent velocity, enthalpy, or concentration, while Γ, S^{ϕ}, and I^{ϕ} represent the diffusion coefficient, the source term, and the interfacial exchange, respectively. A complete set of the governing conservation equations is given in Table 1.

The modeling of the constitutive relations that are needed to close the set of two-phase conservation equations is still in the developing stages. The necess-

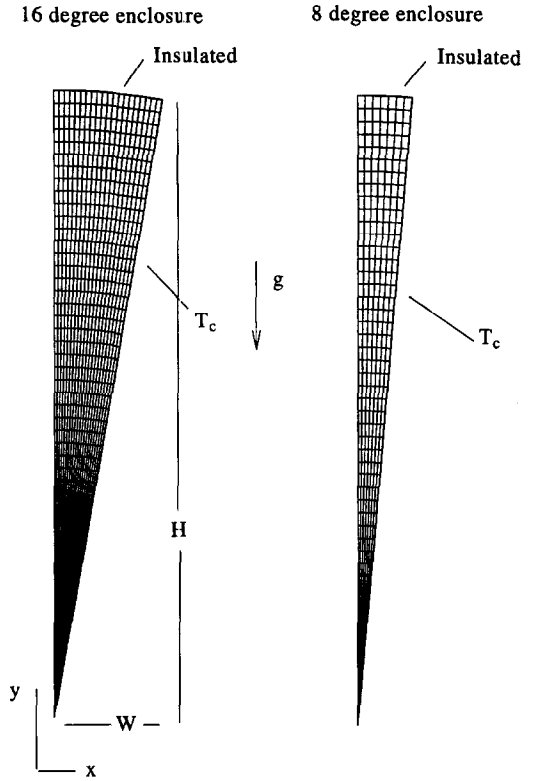

Fig. 1. Physical system, computational grid, and nomenclature relevant to solidification in a V-shaped enclosure.

Table 1. Summary of conservation equations for alloy solidification

Mass conservation:

$$\frac{\partial}{\partial t}(\rho_l r_l)+\nabla\cdot(\rho_l r_l u_l) = -\dot{m}$$

$$\frac{\partial}{\partial t}(\rho_s r_s)+\nabla\cdot(\rho_s r_s u_s) = \dot{m}$$

Momentum conservation:

$$\frac{\partial}{\partial t}(\rho_l r_l u_l)+\nabla\cdot(\rho_l r_l u_l u_l) = r_l\nabla p+\nabla\cdot(\mu_l r_l\nabla u_l)+S_l^u+I_l^u$$

$$\frac{\partial}{\partial t}(\rho_s r_s u_s)+\nabla\cdot(\rho_s r_s u_s u_s) = -r_s\nabla p+\nabla\cdot(\mu_s r_s\nabla u_s)+S_s^u+I_s^u$$

Energy conservation:

$$\frac{\partial}{\partial t}(\rho_l r_l h_l)+\nabla\cdot(\rho_l r_l u_l h_l) = \nabla\cdot\left(\frac{k_l}{C_l}r_l\nabla h_l\right)+S_l^h+I_l^h$$

$$\frac{\partial}{\partial t}(\rho_s r_s h_s)+\nabla\cdot(\rho_{sl} r_s u_s h_s) = \nabla\cdot\left(\frac{k_s}{C_s}r_s\nabla h_s\right)+S_s^h+I_s^h$$

Species conservation:

$$\frac{\partial}{\partial t}(\rho_l r_l c_l)+\nabla\cdot(\rho_l r_l u_l c_l) = \nabla\cdot(r_l\rho_l D_l\nabla c_l)+S_l^c+I_l^c$$

$$\frac{\partial}{\partial t}(\rho_s r_s c_s)+\nabla\cdot(\rho_s r_s u_s c_s) = \nabla\cdot(r_s\rho_s D_s\nabla c_s)+S_s^c+I_s^c$$

ary relations of the model describing alloy solidification have recently been reviewed in the literature [5, 6]. Interfacial exchange relations are necessary to model the interactions between the solid and liquid phases through linking the micro and macro scale physical phenomena. The terms I_l^ϕ and I_s^ϕ are the generalized interfacial exchange coefficients of the variable ϕ. The terms ϕ_s^i and ϕ_l^i are the specific values of the quantity ϕ at the interface for each phase. The terms H_s^ϕ and H_l^ϕ are the diffusional exchange coefficients for the solid phase and the interface and the liquid phase and the interface, respectively. The exchange of ϕ can be expressed as:

$$I_l^\phi = [-\dot{m}_a\phi_l^i+H_l^\phi(\phi_l^i-\phi_l)]A^i \tag{3}$$

$$I_s^\phi = [\dot{m}_a\phi_s^i+H_s^\phi(\phi_s^i-\phi_s)]A^i \tag{4}$$

where $\dot{m}_a$ is the volumetric mass transfer between phases; ϕ_l and ϕ_s are the local values of the phase variable; and A_i is the interface area per unit volume. The interfacial balance, in the absence of an interfacial source term, is given by:

$$I_l^\phi = -I_s^\phi \tag{5}$$

which states that the amount of ϕ entering one phase must be equal to the amount leaving the other phase. The interfacial area, A_i, depends on the morphology of the microstructure of the alloy. For the present study, A_i is determined from the dimensions of the dendritic crystals arm spacing (DAS).

Finally, the interfacial diffusion exchange coefficients need to be defined. The form of H^ϕ can be modified to accommodate the nature of the diffusion of the system under analysis. Furthermore, the transfer coefficient is greatly affected by the microscale morphology of each phase. In dendritic solidification, a solid–liquid microstructure exists within each dendrite where H^ϕ should be considered an effective diffusional exchange coefficient that can account for effective solid–liquid contact areas and tortuosity [7].

When ϕ represents velocity, H_s^ϕ and H_l^ϕ represent the frictional drag coefficient between each phase and the respective interface. The modeling of these terms requires experimental calibration to link the drag coefficients to microstructural parameters. Currently, the manner in which different length scales can be combined into a single drag model is not well understood. However, Ni [8] proposed a generalized drag model such that:

$$H_s^\phi = \frac{3}{4}\frac{\varepsilon_s}{d_s}\rho_l C_{d\varepsilon}|u_l^i-u_s^i|(u_l^i-u_s^i) \tag{6}$$

$$H_l^\phi+\varepsilon_l\nabla(p_l) \tag{7}$$

where ε_s is the solid fraction; d_s is the mean particle length, which is found from A_i; and $C_{d\varepsilon}$ is the gencralized drag coefficient defined as:

$$C_{d\varepsilon} = \frac{24\times 2zq^2(1-\varepsilon_l)}{Re}+C_l q^3 \tag{8}$$

where zq^2 and C_1q^3 are the modified Kozeny factor and inertial contribution coefficients, respectively.

When ϕ represents enthalpy, H_s^ϕ and H_l^ϕ are related to the heat transfer coefficient of each phase and the interface. Likewise, when ϕ represents the concentration, H_s^ϕ and H_l^ϕ are related to the mass transfer coefficient of the interface exchange. The modeling of these terms is analogous when using dimensionless parameters such as the Nusselt (Nu) and Sherwood (Sh) numbers. A generalized expression was developed by Rowe and Claxton [9] to estimate the heat or mass convective transfer coefficient for the interfacial exchange. The equations posited for the liquid phase take the form of:

$$Nu(Sh) = \frac{2}{1-.3(1-\varepsilon_l)} + \frac{2}{3\varepsilon_l} Re^a Pr^3 (Sc^3) \quad (9)$$

where Re is the multiphase Reynolds number given by:

$$Re = \frac{\varepsilon_l |(u_l - u_s)| d_s \rho_l}{\mu_l}. \quad (10)$$

For the solid phase, the heat or mass transfer equations are controlled by diffusion length models. A complete derivation and justification of these models can be found in ref. [10]. It should be noted, moreover, that a considerable amount of experimental verification is necessary to validate the representation of all the interfacial exchange models presented throughout this study.

The thermophysical relations for the two-phase model are consistent with Voller and Prakash [11] with the exception of the addition of the solid-phase relations and the interfacial values of the enthalpy. The expression of the interfacial enthalpy is given by:

$$h_l^i = C_{pi} T^i + L \quad (11)$$

$$h_s^i = C_{ps} T^i. \quad (12)$$

The model accounts for the possibility of locally different liquid and solid temperatures. However, at the interface the enthalpy must share the same value as temperature. The derivation of the expressions regarding enthalpy and temperature are for constant specific heats. This approximation for metal alloys greatly simplifies the mathematical derivation of such terms and, hence, the computational power required to solve the conservation equations.

The enthalpy–temperature relations in the two-phase model are consistent with Voller and Prakash [11] with the addition of an expression for the interfacial value of the solid and liquid concentration. The equations for these values are given as:

$$c_l^i = \frac{c_e(T_m - T^i)}{(T_m - T_e)} \quad (13)$$

$$c_s^i = k_p c_l^i \quad (14)$$

where k_p is the equilibrium partition ratio which can be replaced with the segregation coefficient, κ, when local thermal equilibrium is not imposed on the system. It should also be noted that the phase diagram for the mixture was linearized so that a partition constant could be found. The thermophysical variables of aluminum–copper (Al–Cu) used during all simulations are given in Diao and Tsai [12].

3. NUMERICAL PROCEDURE

The conservation equations were derived to be valid in the fully solid, mushy, and bulk liquid regions, which allow the computational space to be described on a fixed grid. No interface tracking of the mushy region is needed which further allows the variables to be solved using single-domain numerical procedures [13]. A numerical finite-difference scheme was chosen to solve the coupled elliptic partial differential equations governing the flow situation. This method has been tested and verified both in single and binary solidification systems [14–17]. The numerical algorithm chosen employs a control volume based finite difference method (CVFDM) to solve the physical variables on a staggered grid arrangement. The commercial CFD code PHOENICS was used in the current study, which features the inter-phase slip analyzer (IPSA) algorithm. The algorithm was used for the pressure-velocity coupling and the calculations of the phase volume fraction during the simulations [18].

Calculations were performed for a symmetric half plane of a V-shaped geometry for two different angles, 8 and 16°. The polar coordinate system was applied to generate the mesh. Due to the complexity of the point discontinuity at the bottom of the enclosure, a non-uniform grid that was biased at the base of the sump was used. The grid evaluation of the 16° sump started with a uniform grid of 10×20. This grid was far too coarse to provide an accurate description of the flow field, particularly near the discontinuity at the bottom of the sump. A more refined grid of 20×50 corrected the problems associated with the coarse grid. This grid accommodated the stream wise variations in the dependent variables and was numerically stable at greater time steps. A final grid of 30×60 was tested and showed greater refinement; however, the computation time needed to reach convergence was greatly increased. This increase in CPU time led to all simulations being run with a non-uniform 20×50 polar grid for the 16° half plane cases.

The calculations performed in the 8° sump suffered considerably more geometric effects and, hence, needed more grid refinement in the vertical direction. An initial grid of 5×40 was chosen. This grid converged quickly but lacked the necessary resolution to describe the intrigues of the flow field. An increase in the number of vertical grid lines was necessary to provide the resolution not apparent in the 5×40 grid. When considering accuracy and computational time, the best choice of the grid size for the 8° sump was 7×50.

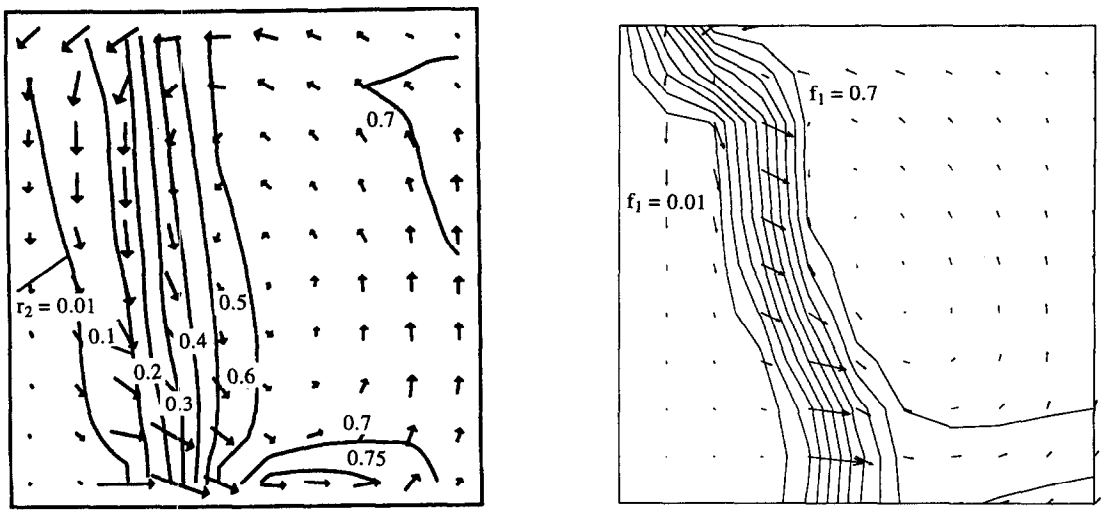

Fig. 2. Comparison of numerical simulations with ref. [15].

A uniform time step of $\Delta t = 0.01$ s was used for both sets of simulations. The highly nonlinear coupling of the dependent variables prevented a larger time step to be used. For a single time step to converge, it took approximately 300 s of CPU time on a dual RISC 6000 processor workstation. False time step under-relaxation was used for the velocity, enthalpy, and concentration. A line-by-line solver was used to obtain converged solutions of the field variables. Each time step was converged when the normalized residuals fell below 10^{-6}, which occurred within 200 line sweeps of the solver.

Effort was made to justify the numerical results obtained during the current study. Comparisons of macrosegregation profiles were obtained between the current study and in work done by Prakash [15] for a binary mixture in a square cavity. The results at 250 s are shown in Fig. 2. The prediction is in agreement. However, slight differences are noticeable, primarily due to the definition of the heat–mass convective transfer coefficient for interfacial exchange and the different generalized drag coefficient used in the current study. The cohesion between the solution methods gives assurance that the current method is numerically accurate in modeling the solidification process in metal alloys.

4. RESULTS AND DISCUSSION

Convection conditions are shown in Figs (3)–(8), which illustrate the velocity vectors, isotherms and concentration profiles of the enclosure ($T_w = 800$K; $T_o = 930$K; $c_{1,0}^{Cu} = 10\%$) during the simulations. A liquidus line ($r_l = 0.8$), which is the boundary between the mushy zone and the bulk liquid region, is represented on each figure representing vectors to distinguish between solid and liquid transport. The vectors indicate that a counter rotating cell, driven by solutal and thermal buoyancy forces, is present after the onset of solidification. The isotherms are plotted in ten equal increments ranging from the minimum and maximum mixture temperature values, and mixture concentrations are plotted in ten equal increments between the minimum and maximum values (expressed in terms of percentage of Cu). In general, the minimum temperature and concentration are found along the outer wall boundary.

4.1. 8° *Enclosure*

The transport associated with an 8° triangular geometry is considered in this work as a limiting size of the liquid pool that forms during continuous casting. Convective heat and mass transfer were hindered due to the large aspect ratio of the enclosure which can significantly limit species redistribution in the melt [19]. The time elapsed before the onset of solidification was approximately 45 s. At 60 s, a mushy region occupied well over one-third of the enclosure. The solid movement in the mushy zone displaced the more dense interdendritic mixture downward, which accounted for the increase in the region near the bottom of the enclosure. The increase of Cu-enriched fluid lowered the liquidus temperature; consequently, the solid growth was slowed. A band of negative segregation developed in the mushy zone due to thermal and solutal forces present in the liquid and two-phase regions. The variation of the mixture concentration averaged 5.4%, with a minimum of 7.1 and a maximum of 12.5%. At 60 s, the isotherms shown in Fig. 3(c) at 60 s showed the distinction of the two regions, two-phase and liquid. The top three isotherms comprised a region where the heat transfer was dominated by the convection in the liquid pool, while the isolines indicate that the latent heat was removed through conduction in the mushy region. This pattern is further depicted by the vectors shown in Fig. 3(b). The liquid velocity drove only superficially into the mushy region, which was slightly less than half the centerline dimension. Therefore, in the two-phase region, conduction is a significant mode of heat trans-

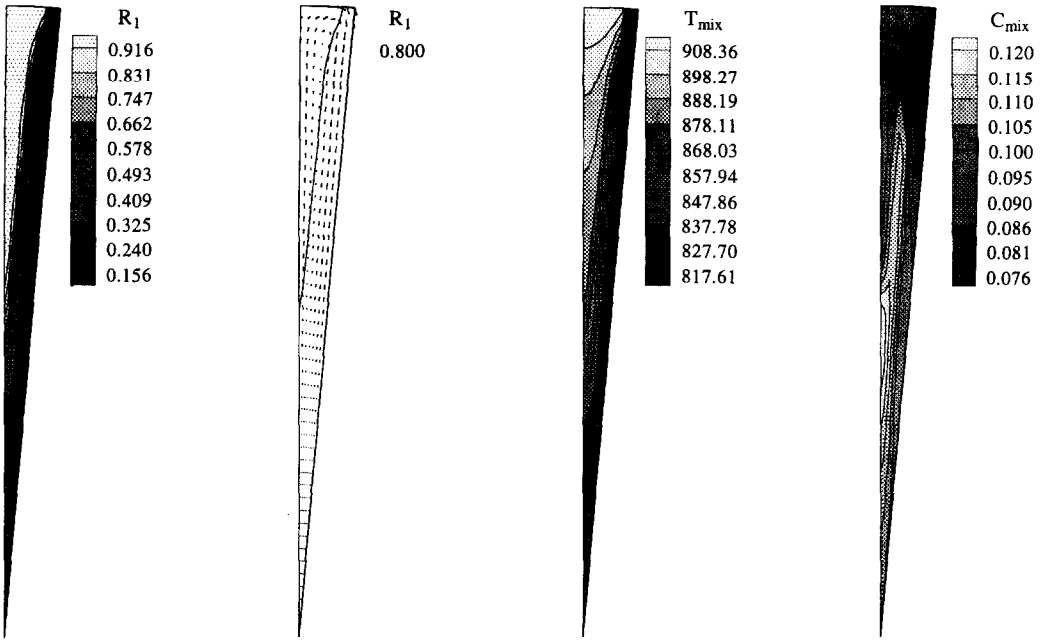

Fig. 3. Liquid fraction, velocity vectors, mixture temperature and concentration for 8° simulation at 60 s.

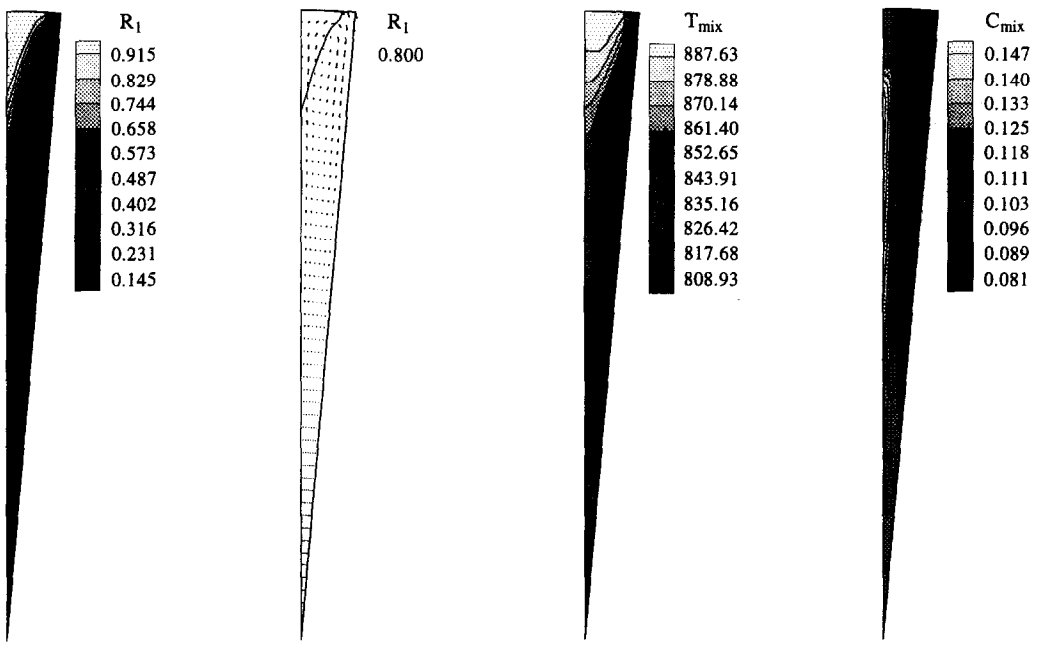

Fig. 4. Liquid fraction, velocity vectors, mixture temperature and concentration for 8° simulation at 90 s.

fer in the 8° enclosure even during the initial periods of solidification.

The convective conditions of the enclosure at a time step of 90 s are shown in Fig. 4. Convection in the liquid pool slowed owing to the large decrease in the dimensions of the remaining fully liquid region from 60 to 90 s. The velocity vectors continued to exhibit a well-defined clockwise rotation due to thermal advection, which was aided by the solutal density variation caused by the increasing vertical mushy zone. It can be observed that the effect of the solutal buoyancy force has grown with respect to the previous time step due to the increase of mixture concentration. At 90 s, the largest values of copper (c_{mix} = 15.6%) were found along the vertical centerline, in the bottom of the liquid pool, and throughout the mushy region. The negative segregation band found after time step 60 s has grown in magnitude and overall geometric size. Two large sections of minimal concentration (c_{mix} = 7.4%) existed along the upper sections of cold walls, which, as a result of raising the solidification temperature, were nearly fully solidified (r_l = 0.06) at

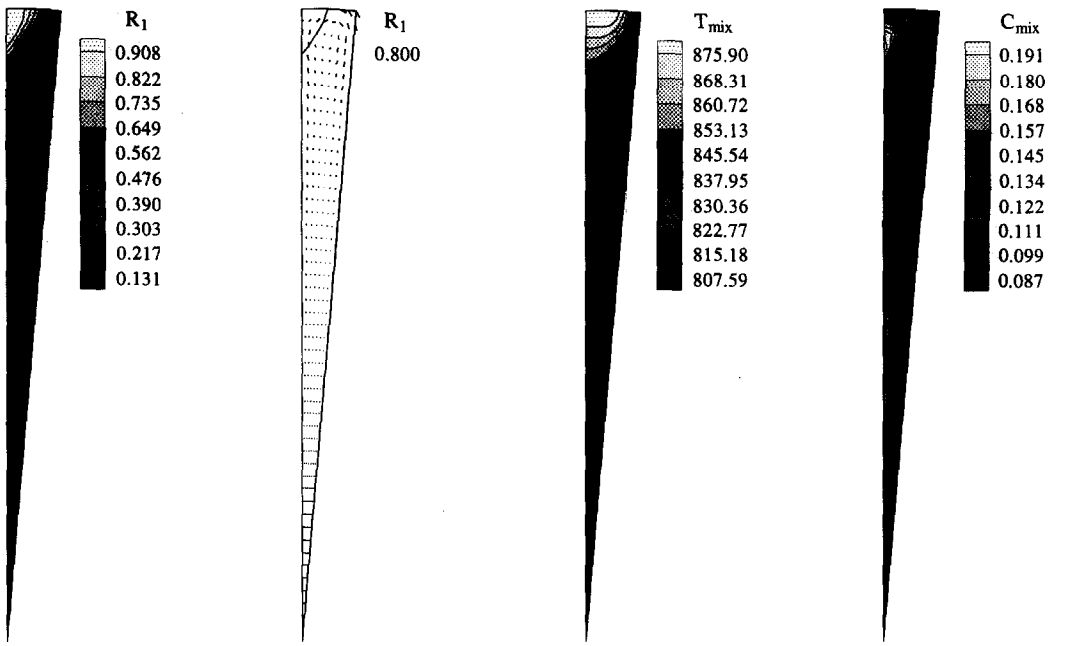

Fig. 5. Liquid fraction, velocity vectors, mixture temperature and concentration for 8° simulation at 120 s.

a higher temperature than in the lower regions of the sump. Within the 30 s between the 60- and 90-s time steps, a significant amount of the enclosure developed a solid front. This front reduced the convective flow, as previously mentioned [see Figs. 3(b) and 4(b)]; however, due to conduction in the metal, the maximum mixture temperature decreased from 919 to 896K.

A final step of 120 s was simulated to demonstrate the increasing severity of the macrosegregation due to limited convection in the enclosure. As can be seen in Fig. 5, the maximum amount of copper reached 21.0%, whereas the minimum decreased to 7.0%. As the negative segregation band in the mushy zone continued to progress upward, it was replaced in the solidified region by a positive segregation band. The isotherms present in the remaining liquid indicate that the heat transfer by convection was largely replaced by conduction throughout the liquid, mushy, and solid regions of the alloy. This enhanced heat removal allowed for an increase in the horizontal thickness of the two-phase region, as depicted in Fig. 5(a). Through 120 s, most of the enclosure was occupied by a solid fraction greater than 0.3, with a large section of nearly solidified metal forming along the cold walls. This time interval was not large enough to provide greater insight into the final macrosegregation patterns that develop in the alloy; nonetheless, the interval was sufficient to provide an understanding of the transport phenomena associated with the 8° enclosure.

4.2. 16° *Enclosure*

As can be observed in Fig. 6, once cooling initiated on the outer wall boundary, a thermal cell developed in the bulk fluid, driven by the downward flow of cooler, dense fluid at the cold boundary. After 90 s of cooling a mushy zone formed, as seen in Fig. 6, with the liquids' interface growing upwards on the cold wall and outward into the melt pool. The nonuniformity of the mushy zone was further increased owing to the effects of solid movement throughout the mushy zone. The developing solid continued to expel Cu-rich fluid, which enriched the interdendritic liquid. In turn, the enriched fluid induced solutal buoyancy forces to act downward on the interdendritic zone. These solutal buoyancy forces aided the thermally driven convective cell because the density of copper was significantly higher than that of aluminum. The mixture concentration varied from 6.5 to 14.2% throughout the mushy zone, as shown in Fig. 6(d), which illustrates the movement of the Cu-rich fluid toward the bottom center of the enclosure. The isotherms varied from 814 to 929K, though the maximum values of mixture temperature were confined to the uppermost section of the enclosure.

As the solid front progressed, into the melt, the geometric properties of the caster walls began to affect the convective transport, as depicted in Figs. 7(a)–(d). At 120 s, the mushy zone adjacent to the cold wall was approaching a fully solidified state ($r_l = 0.03$). The solutal and thermal buoyancy-driven flow as well as the shape of the mold contributed to the thickening of the mushy zone in the middle of the enclosure. The mushy–liquid interface was still approximating the geometric angle of the cast walls. The bottom of the liquidus line is narrowing due to the increased development of the solid front. The mushy zone was considerable wider along the vertical centerline than in the horizontal direction as a result of the accumulation

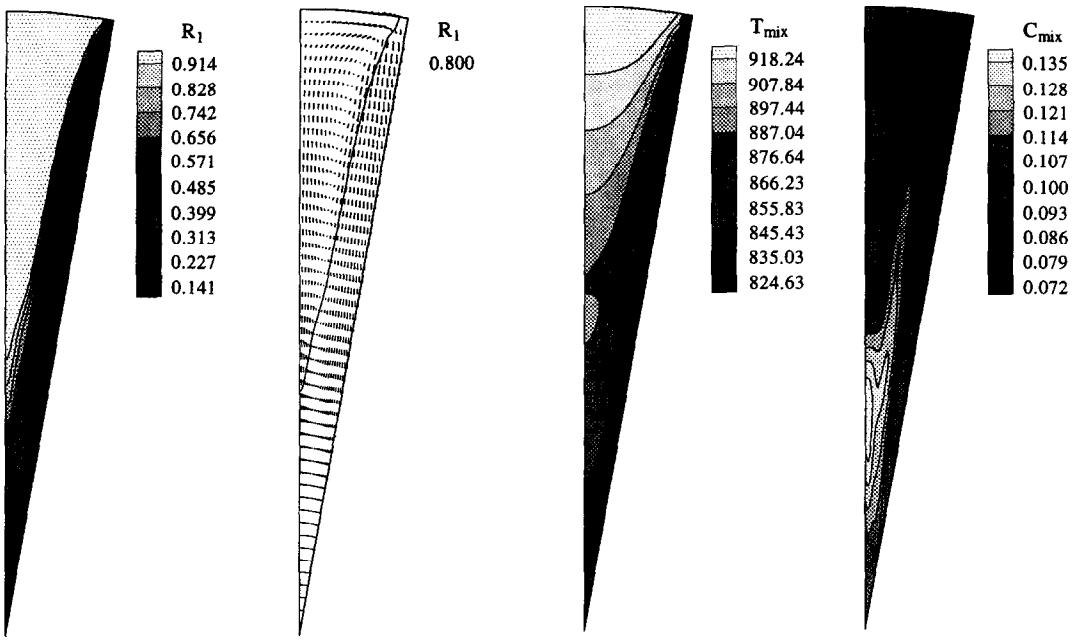

Fig. 6. Liquid fraction, velocity vectors, mixture temperature and concentration for 16° simulation at 90 s.

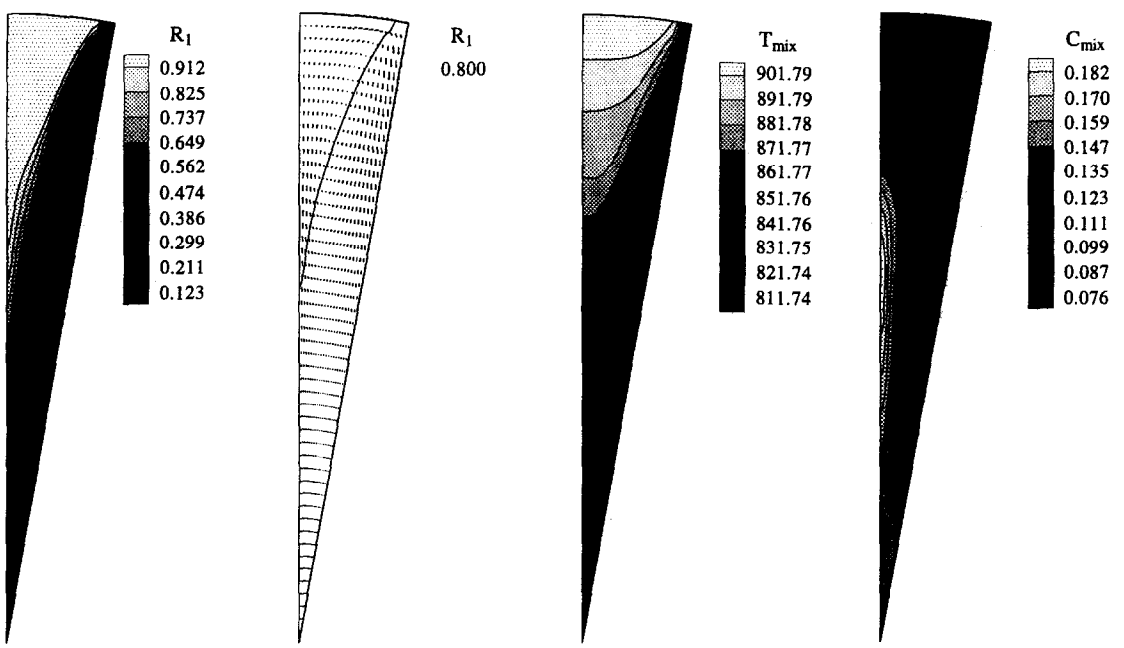

Fig. 7. Liquid fraction, velocity vectors, mixture temperature and concentration for 16° simulation at 120 s.

of Cu-rich interdendritic fluid, which decreased the solidification range of the mixture. Localized remelting occurred within these areas as the solid continued to reject a high-solute mixture in the mushy zone. The mixture concentration of copper varied from a minimum of 6.0% near the upper cold wall to a maximum of 19.0% in the centerline mushy zone. This constituted an increase of approximately 5.0% from 90 s to 120 s. The concentration in the melt ($r_l = 1$) increased from the initial value of 10% to 18% as a maximum near the centerline liquidus interface. With the increase of the solid front, the strength of the thermal convective cell was suppressed. This decrease in convection signifies a possible decrease in significant species redistribution throughout the enclosure. At 120 s, the isotherms indicated that most of the initial preheat of the liquid had been removed through convection in the liquid pool. The large value of solid thermal conductivity ($k_s = 153$ Wm K^{-1}) in the Al–Cu alloy allowed for an additional heat rejection

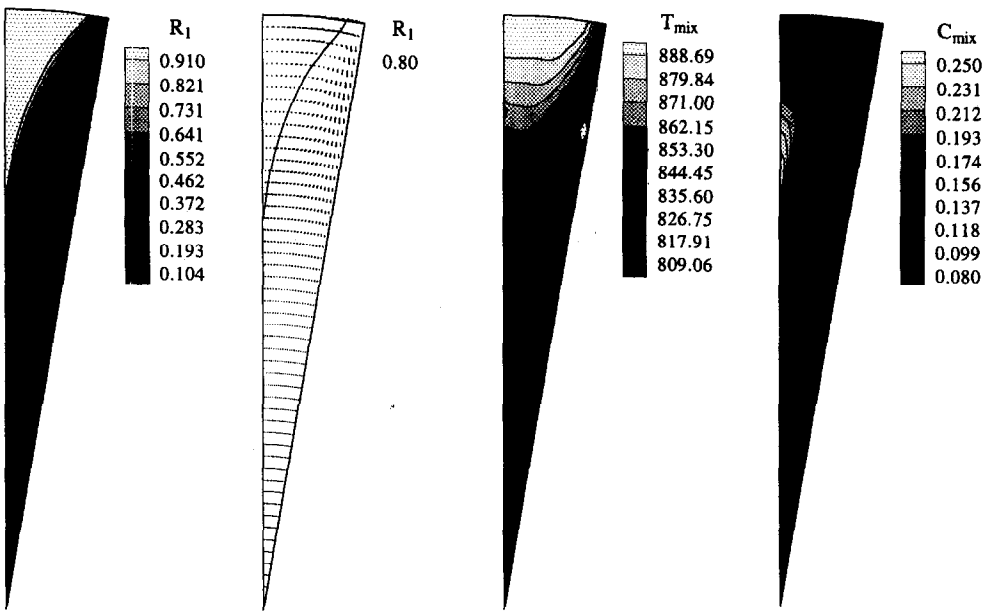

Fig. 8. Liquid fraction, velocity vectors, mixture temperature and concentration for 16° simulation at 150 s.

through the solid as the thermally driven convection slowed. The maximum value of the mixture temperature dropped 17K in the 30-s interval from 929 to 912K, and the solid nearest the cooling wall reached within 2K of the wall temperature.

As convection in the liquid pool decreased, the advancement of the solid front slowed. At 150 s, the angle of the remaining melt widened to approximately 20° (see Fig. 8), which illustrates that the continued downward movement of both solid and Cu-rich fluid was depleting the growth of the upper sections adjacent to the cold walls. A significant amount of the alloy was fully solidified ($r_l \approx 0$). However, due to the large increase of mixture concentration near the center of the enclosure, a mushy region still existed, penetrating deeply along the vertical centerline. The concentration in the fully solid region varied between 6.0 and 10.0%, while in the mushy zone a variation of up to a 17.0% was predicted to occur with percentages of Cu reaching as high as 29.0. As can be seen in Fig. 8, between 90 and 120 s, the maximum mixture temperature dropped from 912 to 893K. This can be attributed to the decrease in melt convection. This decline in convection allowed increased heat transfer through the solid, which was enhanced due to thermal conductivity.

The vectors near the fully solidified region, where, by definition, the solid and liquid velocities are zero, were slightly deflected toward the centerline, causing non-uniformity to develop, as shown in Fig. 8(b). This non-uniformity was strongly related to the movement of interdendritic fluid through the mushy region.

4.3. *Effects of the angle*

The simulations of the solidification process in two limiting cases have shown that different methods of transport may dominate in the sump, depending on the enclosure's geometric parameters. In general, as the aspect ratio of the triangular enclosure increases (i.e. the angle decreases), significant changes occur in the thermal and solutal patterns. During the solidification process in the 8° enclosure, the decrease in convection through the liquid pool leads to an increase in heat transfer via conduction, which is not found to be as pronounced in the 16° geometry. Furthermore, as the magnitude of thermal and solutal convective cells decreases, the formation of negative-banded macrosegregation increases through the mushy zone. Figures 5(d) and 8(d) show the maximum values of mixture concentration for each simulation. While the maximum value is lower in the 8° case, the relative segregation is larger due, we reason, to the fact that the physical dimensions of the enclosure are approximately half the size of the larger domain. The increase of non-homogeneity can be related directly to a change in the dominating method of thermal and solutal transport. As conduction becomes the primary method of heat removal, species redistribution in the liquid and mushy zone is suppressed, which accounts for the severity of the segregated bands.

5. CONCLUSIONS

A two-phase model for momentum, energy, and species transport during alloy solidification has been used to simulate the phase-change process of an Al–Cu alloy in varying geometric enclosures. The effects of the angle of the triangular mold have been included in the simulations. The results indicate that different modes of thermosolutal transport become dominant depending on the angle, which, in turn, affects species redistribution in the forming alloy.

Thermal advection causes stratification to occur in

the molten liquid before the onset of solidification. Consequently, a non-uniform mushy region develops along the cold walls. The subsequent expulsion of a denser Cu-enriched mixture from the advancing solid causes negative banding to occur within the growing mushy zone. Convection in the liquid and through the mushy zone attempts to redistribute the species; however, it is shown that by varying the angle of the enclosure, this movement can be limited.

The limiting cases for liquid pool geometries are simulated, and although the thermosolutal convective patterns during the beginning of the cases are consistent, a transition to conduction driven heat transfer is noted to occur in the 8° enclosure. The different modes of transport affect the macrosegregation of the alloy. The modeling of solid movement in the mushy zone is also attributed to the increasing severity of the segregation. The macrosegregation pattern that forms in each case is characterized by increasing concentrations of Cu with increasing height. Furthermore, the largest amounts of species were found about the centerline of the enclosure for both cases.

In conclusion, as the angle of enclosure decreases, the magnitude of thermosolutal convection and the amount of solute redistribution also decreases. Therefore, to a certain extent, a wider angle in the liquid pool will allow greater potential for solute movement and lessen macrosegregation. The angle of the liquid pool can be controlled by modifying the cooling conditions or by varying the casting speed in the direct chill continuous casting process, resulting in a more homogenous final product. There is a limit, however, as very large ingots are known to have increased macrosegregation in the final cast. This study was intended to investigate geometric effects of the liquid melt pool on solute redistribution and segregation and was not intended to determine the limiting size for the binary mixture. The scope of this work was limited by computational efficiency where future work might include the determination of optimum aspect ratios.

Acknowledgements—The results presented in this paper were obtained in the course of research sponsored by the National Science Foundation (NSF).

REFERENCES

1. Viskanta, R., Mathematical modeling of transport phenomena during solidification of binary systems. In *22nd International Center Heat Mass Transfer Symposium on Manufacturing and Materials Processing*, Yugoslavia, 1990.
2. Beckermann, C. and Viskanta, R., Mathematical modeling of transport phenomena during alloy solidification. *Applied Mechanical Review*, 1993, **46,** 1–25.
3. Burton, R., Dong, Z. and Ebadian, M. A., An experimental investigation of the solidification process in a v-shaped sump. *International Journal of Heat and Mass Transfer*, 1995, **38,** 2383–2393.
4. Wang, C. Y. and Beckermann, C., Multi-scale/-phase modeling of dendritic alloy solidification, HTD-Vol. 284/AMD-Vol. 182, *Transport Phenomena in Solidification*. ASME, 1994, pp. 75–95.
5. Ni, J. and Incropera, F. P., Extension of the continuum model for transport phenomena occurring during metal alloy solidification—I. The conservation equations. *International Journal of Heat and Mass Transfer*, 1995, **38,** 1271–1284.
6. Ni, J. and Incropera, F. P., Extension of the continuum model for transport phenomena occurring during metal alloy solidification—II. Microscopic considerations. *International Journal of Heat and Mass Transfer*, 1995, **38,** 1285–1296.
7. Bird, R. B., Steward, W. E. and Lightfoot, E. N., *Transport Phenomena*. Wiley, New York, 1960.
8. Ni, J., *Development of a two-phase model of transport phenomena during equiaxed solidification*. Ph.D. dissertation, University of Iowa, 1991.
9. Rowe, P. N. and Claxton, K. T., Heat and mass transfer from a single sphere to fluid flowing through an array. *Transactions Chemical Engineers*, 1965, **43,** T321–331.
10. Schneider, M. C. and Beckermann, C., Summary of a method for numerically simulating the columnar dendritic solidification of binary alloys. *Technical Report, UIME-CB*0-1993, Dept of Mechanical Engineering, The University of Iowa, Iowa City, 1993.
11. Prakash, C. and Voller, V. R., On the numerical solution of continuum mixture model equations describing binary solid–liquid phase change. *Numerical Heat Transfer*, 1989, **B**(15), 171–191.
12. Diao, Q. Z. and Tsai, H. L., The formation of negative- and positive-segregated bands during solidification of aluminum–copper alloys. *International Journal of Heat and Mass Transfer*, 1993, **36,** 4299–4305.
13. Patankar, S. V., *Numerical Heat Transfer and Fluid Flow*. Hemisphere, Washington, DC, 1980.
14. Bennon, W. D. and Incropera, F. P., A continuum model for momentum, heat and solute transfer in binary and solid–liquid phase change systems—II. Application to solidification in a rectangular cavity. *International Journal of Heat and Mass Transfer*, 1987, **30,** 2171–2187.
15. Prakash, C., Two-phase model for binary solid–liquid phase change, part II . Some illustrative examples. *Numerical Heat Transfer*, 1990, **B**(18), 147–169.
16. Prescott, P. J. and Incropera, F. P., Numerical simulation of a solidifying Pb–Sn alloy : the effects of cooling rate on thermosolutal convection and macrosegregation. *Metallurgical Transactions B*, 1991, **22**(B), 529–540.
17. Wang, C. Y. and Beckermann, C., A multiphase solute diffusion model for alloy solidification. *Metallurgical Transactions A*, 1993, **24**(A), 2787–2802.
18. Spalding, D. B., Development in the IPSA procedure for numerical computation of multiphase-flow phenomena with interphase slip, unequal temperatures, etc. In *Numerical Properties and Methodologies in Heat Transfer*, ed. T. M. Shin. Hemisphere, New York, 1983.
19. Flemings, M. C., *Solidification Processing*. McGraw–Hill, New York, 1974.